Satellite spectra of heliumlike nickel

H. Hsuan, M. Bitter, K. W. Hill, S. von Goeler, B. Grek, D. Johnson,
L. C. Johnson, and S. Sesnic
Plasma Physics Laboratory, Princeton University, P.O. Box 451, Princeton, New Jersey 08544

C. P. Bhalla and K. R. Karim
Department of Physics, Kansas State University, Manhattan, Kansas 66506

F. Bely-Dubau and P. Faucher
Observatoire de Nice, BP 139, F-06003 Nice Cedex, France
(Received 1 December 1986)

Spectra of heliumlike nickel, Ni XXVII, have been observed from Tokamak Fusion Test Reactor (TFTR) plasmas with a high-resolution crystal spectrometer. The experimental arrangement permits simultaneous observation of the heliumlike resonance line, the intercombination and forbidden lines, and all the associated satellites due to transitions $1s^2nl$-$1s2l'nl''$ with $n \geq 2$. Relative wavelengths and line intensities can thus be determined very accurately. The observed spectral data are in good agreement with results from the present Hartree-Fock-Slater atomic model calculations and predictions from the Z-expansion method.

I. INTRODUCTION

Heliumlike and hydrogenlike spectra of high-Z ions are of interest for the diagnostics of tokamak plasmas and solar flares, and they are also important for the testing of atomic theories which must include relativistic and quantum electrodynamical effects.[1-3] So far, spectra of heliumlike and hydrogenlike ions with $Z \leq 26$, especially Ar, Ti, Cr, and Fe, have been studied in detail from tokamak plasmas.[4-12] With the new generation of tokamaks, e.g., the Joint European Torus[13] (JET) and the Tokamak Fusion Test Reactor[14] (TFTR), which are designed to obtain fusion breakeven, it is possible to maintain plasmas of large volumes ($V > 40$ m^3) with electron densities n_e in the range from 10^{19} to 10^{20} m^{-3} and electron temperatures $T_e > 5$ keV in steady-state conditions for several seconds. Under these conditions, elements with $Z > 26$ can be observed in the heliumlike and hydrogenlike charge states.

In this paper spectra of heliumlike nickel Ni XXVII are presented as well as a detailed comparison of the experimental data with results from Hartree-Fock-Slater atomic model calculations,[15,16] and the results obtained by the Z-expansion method.[17-19] The experimental results are presented in Sec. II. The identification of the observed spectral features and comparison of wavelengths and intensities with theoretical predictions are described in Sec. III. The analysis results and diagnostic applications are discussed in Sec. IV.

II. EXPERIMENT

The measurements have been performed on TFTR with a new crystal spectrometer which consists of three crystals and position-sensitive detectors in the Johann configuration.[20] The instrument has been designed to record spectra from three approximately vertical chords of the plasma minor section in order to measure radial profiles of the ion temperature and plasma rotation velocity from the Doppler broadening and Doppler shift of x-ray lines from metal impurity ions of Ti, Cr, Fe, and Ni. Traces ($\lesssim 0.1\%$) of these elements are present in TFTR plasmas from the Inconel (~ 70 at. % Ni, ~ 15 at. % Cr, ~ 7 at. % Fe, ~ 2.5 at. % Ti) bellow protective plates and the stainless-steel vacuum vessel. The resolution of the spectrometer is $\lambda/\Delta\lambda > 10\,000$. 128 spectra per crystal are recorded during a TFTR discharge for time-resolved measurements of these plasma parameters.[21] The wavelength range obtained with a single spectrometer setting covers the entire spectral range of the dielectronic satellite lines of heliumlike ions. It is thus possible to determine the satellite to resonance line intensity ratios accurately from a *simultaneous measurement of these lines.* This is important for diagnostic applications of these intensity ratios for measurements of the electron temperature, the ionization equilibrium, and ion transport.[9-12]

The nickel spectra were obtained from a central vertical chord (at a major radius $R = 249$ cm) with a (22$\bar{4}$3) quartz crystal ($2d = 2.028$ Å) of the size $1.5 \times 6 \times 0.030$ in.^{3}. The curvature radius was $R_c = 1013$ cm, and the spectral resolution was $\lambda/\Delta\lambda = 18\,000$. Figure 1 shows a measured spectrum of Ni XXVII. The data were obtained

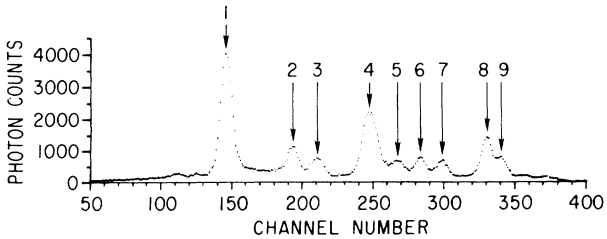

FIG. 1. Satellite spectrum of Ni XXVII. The data were recorded from an ohmically heated TFTR discharge during its steady-state phase.

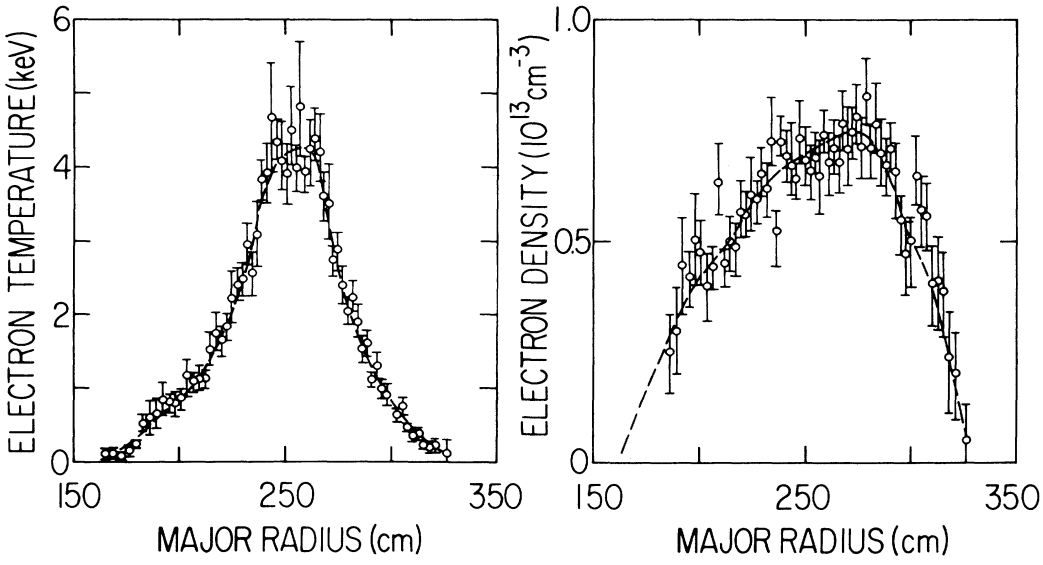

FIG. 2. Radial profiles of the electron temperature and the electron density as measured by the TFTR Thomson scattering diagnostic.

from the steady-state phase of a TFTR discharge with a central electron temperature of 4 keV and a very low central electron density $n_e(0)=8\times10^{12}$ cm^{-3}. The radial profiles of the electron temperature and electron density as measured by laser Thomson scattering are shown in Fig. 2. Under these conditions the plasma electrons and plasma ions are weakly coupled, such that the ion temperature is well below the electron temperature. The spectral features are, therefore, well-resolved and not obscured by Doppler broadening. Moreover, the collisionally excited lithiumlike and berylliumlike satellites are expected to be prominent spectral features, since substantial deviations from coronal equilibrium occur under these experimental conditions.[22]

III. LINE IDENTIFICATION

The nine prominent features of the spectrum shown in Fig. 1 have been identified as the resonance line, the intercombination lines, and the forbidden line of heliumlike nickel Ni XXVII and the associated strong lithiumlike and berylliumlike satellites of the resonance line. The transitions of these spectral features are listed in Table I. The key letters correspond to Gabriel's notation.[23] Also listed in Table I are the theoretical wavelengths and line strengths $F_2(sf)$ for the strong dielectronic satellites as obtained by Vainshtein and Safronova[17,18] and from our present calculations which are described below. The channel numbers N in column 4 of Table I correspond to the center positions of the observed spectral features. They were obtained from a least-mean-squares fit of Voigt functions, and they were then used for determination of the experimental wavelengths using the following relation:

$$\lambda=2d\sin(\theta_0+\Delta\theta)\ , \tag{1}$$

where $\Delta\theta$ (degree) $=3.719\times10^{-3}$ $(N\text{-}N_0)$ corresponds to the dispersion of the instrument. N_0 is the center channel number of peak 1. Since the spectrometer is not absolutely calibrated, the experimental wavelengths are given in reference to the theoretical wavelength values for the resonance line w by assigning $\lambda_w^{\text{theor}}=2d\sin\theta_0$ to the center channel N_0 of peak 1. We note from Table I that both sets of theoretical wavelengths are in good agreement with the experimental values. For a more detailed comparison between theory and experiment synthetic spectra were constructed from the theoretical transition arrays in Table I as well as from the transition arrays for the $n=3,4$ lithiumlike satellites, which are given in Table II and in Ref. 19. To facilitate a direct comparison with the experimental data, channel numbers were converted into wavelengths by using Eq. (1), and Voigt functions were then calculated from the theoretical transitions for this wavelength array. The synthetic spectra are shown in Figs. 3 and 4 together with the experimental data. The calculated contributions from the different spectral components, i.e., the heliumlike lines, the dielectronic lithiumlike satellites, and the collisionally excited lithiumlike and berylliumlike satellites, to the total synthetic spectrum are shown separately by the shaded areas in Figs. 3(b)—3(d) and 4(b)—4(d). The line intensities of the synthetic spectrum were normalized to the intensity of the resonance line w. The intensities of the heliumlike lines x, y, and z were obtained from the following expression:

$$\frac{I_{x,y,z}}{I_w}=\frac{C_{x,y,z}(T_e)}{C_w(T_e)}\ . \tag{2}$$

TABLE I. Experimental wavelengths and theoretical predictions for the resonance, intercombination, and forbidden lines of Ni XXVII, and the associated satellite lines due to transitions $1s^2 2l - 1s\,2l'2l''$. Wavelengths are in Å and satellite line strengths $F_2(sf)$ are in units of 10^{13} s^{-1}.

Peak	Key	Transition	N	λ_{expt}	λ_{theor}[b]	F_2[b](sf)	λ_{expt}	λ_{theor}[c]	F_2[c](sf)
1	w	$1s^2\,{}^1S_0 - 1s\,2p\,{}^1P_1$	146.11	1.5879[a]	1.5879		1.5886[a]	1.5886	
2	x	$1s^2\,{}^1S_0 - 1s\,2p\,{}^3P_2$	193.18	1.5917	1.5918		1.5924	1.5925	
	s	$1s^2 2s\,{}^2S_{1/2} - 1s\,2s\,2p\,{}^2P_{3/2}$			1.5926	0.0106		1.5935	2.40
	b	$1s^2 2p\,{}^2P_{1/2} - 1s\,2p^2\,{}^2P_{3/2}$			1.5929	0.157			
3	m	$1s^2 2p\,{}^2P_{3/2} - 1s\,2p^2\,{}^2S_{1/2}$	210.21	1.5931	1.5932	6.00	1.5938	1.5940	4.98
	t	$1s^2 2s\,{}^2S_{1/2} - 1s\,2s\,2p\,{}^2P_{1/2}$			1.5934	12.8		1.5940	11.12
4	y	$1s^2\,{}^1S_0 - 1s\,2p\,{}^3P_1$	248.04	1.5962	1.5959		1.5969	1.5968	
	q	$1s^2 2s\,{}^2S_{1/2} - 1s\,2s\,2p\,{}^2P_{3/2}$			1.5965	0.472		1.5972	
	a	$1s^2 2p\,{}^2P_{3/2} - 1s\,2p^2\,{}^2P_{3/2}$			1.5973	17.5		1.5981	14.40
5	k	$1s^2 2p\,{}^2P_{1/2} - 1s\,2p^2\,{}^2D_{3/2}$	267.17	1.5978	1.5980	38.1	1.5985	1.5987	39.32
	d	$1s^2 2p\,{}^2P_{1/2} - 1s\,2p^2\,{}^2P_{1/2}$			1.5980	0.166			
6	r	$1s^2 2s\,{}^2S_{1/2} - 1s\,2s\,2p\,{}^2P_{1/2}$	283.50	1.5991	1.5992	6.93	1.5998	1.6003	7.19
7	j	$1s^2 2p\,{}^2P_{3/2} - 1s\,2p^2\,{}^2D_{5/2}$	298.31	1.6003	1.6005	58.0	1.6010	1.6011	53.49
8	l	$1s^2 2p\,{}^2P_{3/2} - 1s\,2p^2\,{}^2D_{3/2}$	330.47	1.6029	1.6024	5.73	1.6036	1.6033	4.84
	z	$1s^2\,{}^1S_0 - 1s\,2s\,{}^3S_1$			1.6031			1.6035	
9	β	$1s^2 2s^2\,{}^1S_0 - 1s\,2s^2 2p\,{}^1P_1$	340.32	1.6037			1.6044	1.6047	

[a]The experimental wavelengths are normalized to the theoretical values for the $1s^2\,{}^1S_0 - 1s\,2p\,{}^1P_1$ transition.
[b]References 17 and 18.
[c]Present HFS calculations.

TABLE II. Atomic data calculated with the HFS atomic model for satellite line transitions: $1s^2 nl - 1s\,2l'nl''$ with $n = 3,4$ of Ni XXVI. The wavelengths are in Å. The line strengths $F_2(sf)$ are in units of 10^{13} s^{-1}. Lines with F_2 values less than 10^{13} s^{-1} are not listed.

Final state $\lvert f\rangle$	Autoionizing state $\lvert s\rangle$	λ (Å)	$F_2(sf)$ (10^{13} s^{-1})
$1s^2 3p\,{}^2P_{3/2}$	$1s\,2p\,({}^1P)3p\,{}^2S_{1/2}$	1.5892	2.66
$1s^2 4p\,{}^2P_{3/2}$	$1s\,2p\,({}^1P)4p\,{}^2P_{3/2}$	1.5897	1.93
$1s^2 4p\,{}^2P_{1/2}$	$1s\,2p\,({}^1P)4p\,{}^2D_{3/2}$	1.5898	4.82
$1s^2 4p\,{}^2P_{3/2}$	$1s\,2p\,({}^1P)4p\,{}^2D_{5/2}$	1.5899	3.94
$1s^2 3p\,{}^2P_{3/2}$	$1s\,2p\,({}^1P)3p\,{}^2P_{3/2}$	1.5903	6.24
$1s^2 3s\,{}^2S_{1/2}$	$1s\,2p\,({}^1P)3s\,{}^2P_{1/2}$	1.5904	1.26
$1s^2 3p\,{}^2P_{1/2}$	$1s\,2p\,({}^1P)3p\,{}^2D_{3/2}$	1.5906	12.82
$1s^2 3p\,{}^2P_{3/2}$	$1s\,2p\,({}^1P)3p\,{}^2D_{5/2}$	1.5912	15.94
$1s^2 4d\,{}^2D_{5/2}$	$1s\,2p\,({}^1P)4d\,{}^2F_{5/2}$	1.5919	1.97
$1s^2 4d\,{}^2D_{3/2}$	$1s\,2p\,({}^1P)4d\,{}^2D_{5/2}$	1.5920	1.07
$1s^2 4d\,{}^2D_{5/2}$	$1s\,2p\,({}^1P)4d\,{}^2F_{7/2}$	1.5922	5.05
$1s^2 3p\,{}^2P_{3/2}$	$1s\,2p\,({}^3P)3p\,{}^2D_{5/2}$	1.5936	1.86
$1s^2 3d\,{}^2D_{3/2}$	$1s\,2p\,({}^1P)3d\,{}^2F_{5/2}$	1.5951	3.36
$1s^2 3d\,{}^2D_{5/2}$	$1s\,2p\,({}^1P)3d\,{}^2F_{5/2}$	1.5956	3.09
$1s^2 3d\,{}^2D_{5/2}$	$1s\,2p\,({}^1P)3d\,{}^2F_{7/2}$	1.5963	9.98
$1s^2 3s\,{}^2S_{1/2}$	$1s\,2p\,({}^3P)3s\,{}^2P_{1/2}$	1.5966	5.09
$1s^2 4p\,{}^2P_{3/2}$	$1s\,2p\,({}^3P)4p\,{}^2D_{3/2}$	1.5975	1.03
$1s^2 4p\,{}^2P_{3/2}$	$1s\,2p\,4p\,{}^4D_{5/2}$	1.5980	1.67
$1s^2 3p\,{}^2P_{3/2}$	$1s\,2p\,3p\,{}^4D_{5/2}$	1.5997	2.33
$1s^2 4s\,{}^2S_{1/2}$	$1s\,2p\,({}^3P)4s\,{}^2P_{1/2}$	1.6032	1.01
$1s^2 3p\,{}^2P_{3/2}$	$1s\,3s\,({}^3S)2s\,{}^2S_{1/2}$	1.6050	1.41

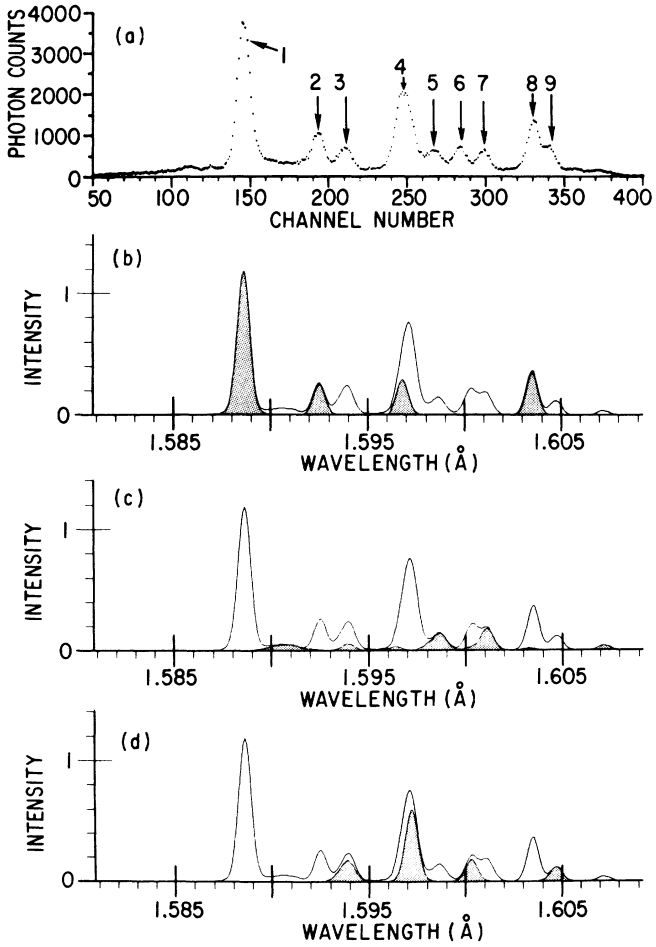

FIG. 3. Comparison of the observed Ni XXVII spectrum with a synthetic spectrum constructed from the results obtained by the present HFS atomic model calculations. The experimental data are shown in (a). The contributions from the heliumlike lines, the dielectronic lithiumlike satellites, and the collisionally excited lithiumlike and berylliumlike satellites to the synthetic spectrum are shown by the shaded areas in (b), (c), and (d), respectively. The envelope shown in (b), (c), and (d) is the total synthetic spectrum, i.e., the sum of the various components.

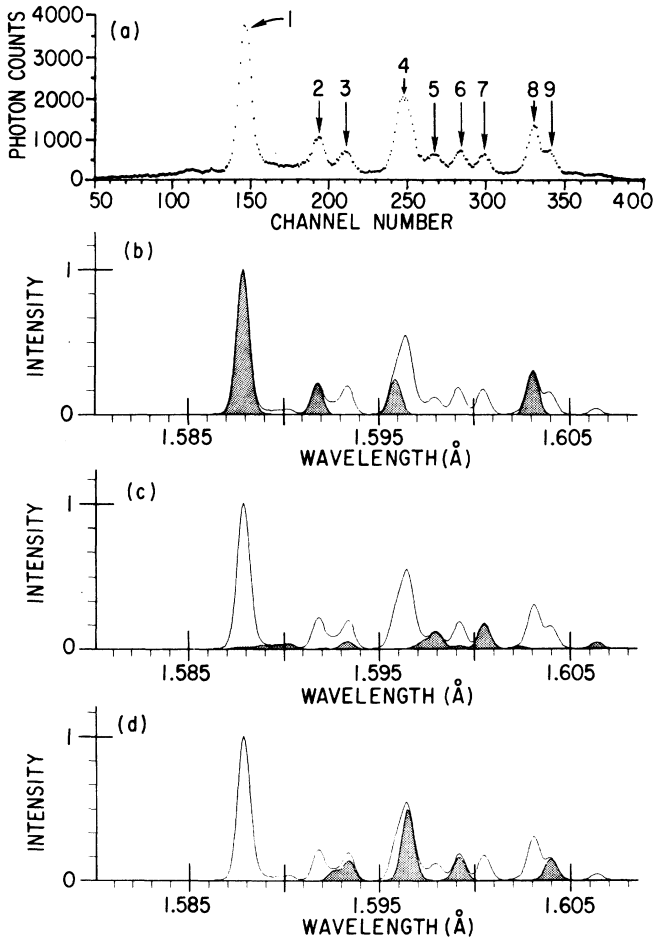

FIG. 4. Comparison of the observed Ni XXVII spectrum with a synthetic spectrum calculated from the theory of Vainshtein and Safronova (Refs. 17–19). The experimental data are shown in (a). The contributions from the heliumlike lines, the dielectronic lithiumlike satellites, and the collisionally excited lithiumlike and berylliumlike satellites to the synthetic spectrum are shown by the shaded areas in (b), (c), and (d), respectively. Also shown in (b), (c), and (d) is the total synthetic spectrum, i.e., the sum of the various components.

Values for the excitation rate coefficients $C_{x,y,z,w}$ were calculated using the methods described in Refs. 7 and 9. Here, we included only the contributions from direct excitation, radiative cascade transitions, and collisional resonances, but we neglected the contribution to the line z from the inner-shell ionization. The relative intensities for the dielectronic satellites were calculated from the following expression:

$$\frac{I_s^{\text{diel}}}{I_w}=\frac{1}{2C_w(T_e)}\left[\frac{2\pi\hbar^2}{m_e kT_e}\right]^{3/2}F_2(sf)\exp\left[\frac{-E_s}{kT_e}\right] \tag{3}$$

with

$$F_2(sf)=\frac{g_s A_a(s)A_r(sf)}{A_T(s)}\ .$$

$F_2(sf)$ is the satellite line strength; E_s is the Auger electron energy; $A_T(s)$ is the total transition rate of the autoionizing state $|s\rangle$; $A_a(s)$ and $A_r(sf)$ are, respectively, the Auger transition rate to the ground state and the radiative rate of $|s\rangle$ to the final state $|f\rangle$.

In the present calculations, the Hartree-Fock-Slater (HFS) atomic model was employed to obtain the single-particle wave functions. These wave functions were then used to calculate the radial Auger and electric dipole matrix elements. Configuration state functions belonging to the same complex were allowed to mix. The diagonal elements of the energy matrix were corrected for relativistic effects. The effects due to spin-orbit interaction were included. The energy matrices were diagonalized to obtain correlated atomic state functions and energies; these were used in calculating transition rates. For the w, x, y, j, q,

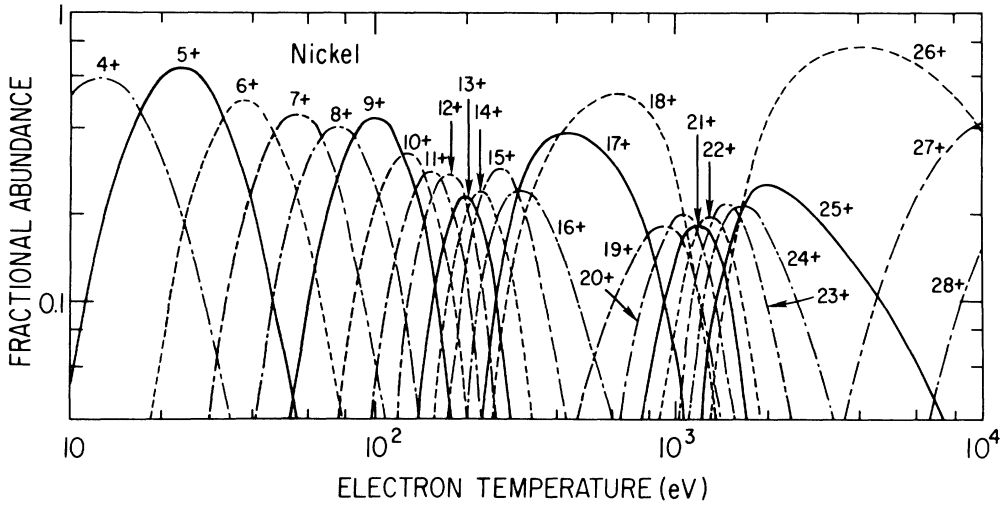

FIG. 5. Fractional abundance of the ionization states of nickel for coronal equilibrium (Ref. 26).

β, and z lines the wavelengths were calculated using the multiconfiguration Dirac-Fock model including radiative corrections of quantum electrodynamics. The difference between the Dirac-Fock wavelength and the Hartree-Fock-Slater wavelength for the j line was 0.0025 Å. This was added to the wavelengths of all other dielectronic satellite lines. The synthetic spectrum shown in Fig. 3 was constructed from the HFS results. In Ref. 17, the Z-expansion method is used to calculate the atomic quantities which were used in the synthetic spectrum shown in Fig. 4.

The intensity of the collisionally excited lithiumlike (berylliumlike) satellites was obtained from the following expression:

$$\frac{I_s^{\text{coll}}}{I_w} = \frac{C_s(T_e)}{C_w(T_e)} \frac{n_{\text{Ni}*}}{n_{\text{Ni XXVII}}} , \tag{4}$$

where $n_{\text{Ni}*}$ ($=n_{\text{Ni XXVI}}$ or $n_{\text{Ni XXV}}$) and $n_{\text{Ni XXVII}}$ are the densities of lithiumlike (or berylliumlike) and heliumlike nickel. $C_s(T_e)$ is the rate coefficient for electron-impact excitation of the lithiumlike (or berylliumlike) ion from the ground state.

The synthetic spectra were calculated for the experimentally observed electron and ion temperatures of $T_e=4$ keV and $T_i=2$ keV, respectively. Values of $n_{\text{Ni XXVI}}/n_{\text{Ni XXVII}}=0.75$ and $n_{\text{Ni XXV}}/n_{\text{Ni XXVII}}=0.1$ for the relative abundance of heliumlike, lithiumlike, and berylliumlike nickel were chosen to obtain a best fit with the observed spectrum.

IV. DISCUSSION

The detailed comparisons shown in Figs. 3 and 4 indicate that the predictions from both theories are in very good agreement with the experiment. The predictions differ only slightly with respect to the wavelength for the satellite r (feature 6), where the value of Vainshtein and Safronova is in somewhat better agreement with the experiment than the value obtained from the present calculations. The predicted intensities for feature 3 are in both cases slightly higher than the observed value.

The observed Ni XXVII spectra confirm the trend of the charge-dependent wavelength shifts reported in Ref. 24. In particular, we observe that the satellite q overlaps with the y line. Similarly, the satellite β is very close to the line z. On the other hand, the dielectronic satellite k and the collisionally excited satellite r are well separated. These charge-dependent wavelength shifts imply that the line q is no longer appropriate for the diagnostic of the relative abundance of the lithiumlike and heliumlike charge states. The satellite r can be used instead.

The values for the abundance of Ni XXV and Ni XXVI relative to that of Ni XXVII, which were obtained from the analysis in Sec. III, are substantially larger than the predictions[25] for the fractional abundance of these charge states in coronal equilibrium (see Fig. 5). Modeling calculations, such as those described in Ref. 9, make it possible to deduce values for the radial ion transport coefficients from these observed deviations. The resonance lines w of Ni XXVII as well as Fe XXV have been successfully used for Doppler measurements. Doppler ion temperatures $T_i > 20$ keV have recently been measured in TFTR experiments with intense neutral beam heating from these impurity lines.[26,27]

Note added in proof. Spectra of Ni XXVII have recently also been observed from JET tokamak plasma [F. Bombarda *et al.* (private communication)].

ACKNOWLEDGMENTS

The technical assistance of J. Gorman, J. Lehner, P. Howard, and the TFTR operating crew is highly appreciated. We also gratefully acknowledge the continuing support of Dr. K. M. Young, Dr. H. P. Furth, Dr. R. Goldston, Dr. D. Grove, Dr. D. M. Meade, and Dr. P. H.

Rutherford. This work was supported by U. S. Department of Energy Contract No. DE-AC02-76-CH0-3073. Two of us (C.P.B. and K.R.K.) were supported by the Division of Chemical Sciences, Office of Basic Energy Sciences, Office of Energy Research, and the U.S. Department of Energy. Computations of excitation rate coefficients were carried out on the NAS 980-CIRCE computer in Orsay, France.

[1]J. Dubau and S. Volonte, Rep. Prog. Phys. **43**, 199 (1980).
[2]C. De Michelis and M. Mattioli, Nucl. Fusion **21**, 677 (1981).
[3]R. K. Janev, L. P. Presnyakov, and V. P. Shevelko, in *Physics of Highly Charged Ions,* Vol. 13 of *Springer Series in Electrophysics,* edited by G. Ecker (Springer, Berlin, 1985).
[4]TFR Group and F. Bombarda, in *Proceedings of the Eleventh Europen Conference on Controlled Fusion and Plasma Physics, Aachen, Federal Republic of Germany, 1983,* edited by S. Methfessel (European Physical Society, Aachen, 1983), Vol. 7D, Part I, p. 89.
[5]TFR Group, F. Bombarda, F. Bely-Dubau, P. Faucher, M. Cornille, J. Dubau, and M. Loulergue, Phys. Rev. A **32**, 2374 (1985).
[6]E. Kallne, J. Kallne, A. Dalgarno, E. S. Marmar, J. E. Rice, and A. K. Pradhan, Phys. Rev. Lett. **52**, 2245 (1984).
[7]F. Bely-Dubau, P. Faucher, L. Steenman-Clark, M. Bitter, S. von Goeler, K. W. Hill, C. Camhy-Val, and J. Dubau, Phys. Rev. A **26**, 3459 (1982).
[8]P. Lee, A. J. Lieber, and S. S. Wojtowicz, Phys. Rev. A **31**, 3996 (1985).
[9]M. Bitter, K. W. Hill, M. Zarnstorff, S. von Goeler, R. Hulse, L. C. Johnson, N. R. Sauthoff, S. Sesnic, K. M. Young, M. Tavernier, F. Bely-Dubau, P. Faucher, M. Cornille, and J. Dubau, Phys. Rev. A **32**, 3011 (1985).
[10]TFR Group, J. Dubau, and M. Loulergue, J. Phys. B **15**, 1007 (1981).
[11]M. L. Apicella, R. Bartiromo, F. Bombarda, and R. Giannella, Phys. Lett. **98A**, 174 (1983).
[12]M. Bitter, K. W. Hill, N. R. Sauthoff, P. C. Efthimion, E. Meservey, W. Roney, S. von Goeler, R. Horton, and W. Stodiek, Phys. Rev. Lett. **43**, 129 (1979).
[13]R. J. Bickerton, Plasma Phys. Controlled Fusion **26**, 1355 (1984).
[14]K. M. Young *et al.*, Plasma Phys. Controlled Fusion **26**, 11 (1984).
[15]C. P. Bhalla and K. R. Karim, Phys. Rev. A **34**, 3525 (1986).
[16]K. R. Karim and C. P. Bhalla, Phys. Rev. A **34**, 4743 (1986).
[17]L. A. Vainshtein and U. I. Safronova, At. Data Nucl. Data Tables **21**, 49 (1978).
[18]U. I. Safronova, A. M. Urnov, and L. A. Vainshtein, Proc. P. N. Lebedev. Phys. Inst. [Acad. Sci. USSR **119**, 13 (1980)].
[19]L. A. Vainshtein and U. I. Safronova, At. Data Nucl. Data Tables **25**, 311 (1980).
[20]H. Johann, Z. Phys. **69**, 189 (1931).
[21]M. Bitter, K. W. Hill, S. Cohen, S. von Goeler, H. Hsuan, L. C. Johnson, R. Raftopulos, M. Reale, N. Schechtman, S. Sesnic, F. Spinos, J. Timerlake, S. Weicher, N. Young, and K. M. Young, Rev. Sci. Instrum. **57**, 2145 (1986).
[22]M. Bitter, S. von Goeler, N. Sauthoff, K. W. Hill, K. Brau, D. Eames, M. Goldman, E. Silver and W. Stodiek, in *Inner-Shell and X-Ray Physics of Atoms and Solids,* edited by D. J. Fabian, H. Kleinpoppen, and L. M. Watson (Plenum, New York, 1981), p. 861.
[23]A. H. Gabriel, Mon. Not. R. Astron. Soc. **160**, 99 (1972).
[24]TFR Group, M. Cornille, J. Dubau, and M. Loulergue, Phys. Rev. A **32**, 3000 (1985).
[25]C. Breton, C. De Michelis, M. Finkenthal, and M. Matioli, Fontenay-aux-Roses Laboratory Report No. EUR-CEA-FC-948, 1978 (unpublished).
[26]H. Hsuan, M. Bitter, S. von Goeler, S. Sesnic, J. Timberlake, and S. Cohen, Bull. Am. Phys. Soc. **31**, 1611 (1986).
[27]M. Bitter, K. W. Hill, S. Hiroe, H. Hsuan, S. von Goeler, S. Sesnic, and M. Zarnstorff, Bull. Am. Phys. Soc. **31**, 1414 (1986).